

Piezoelectric effect on thermoelastic Lamb waves in functionally graded plates

X. WANG, X. REN, J. YU, H. ZHOU, X. ZHANG, J. LENG

School of Mechanical and Power Engineering, Henan Polytechnic University, Jiaozuo 454003, China, Xianhui Wang, e-mail: wxhpu@163.com (corresponding author)

BASED ON THE LORD–SHULMAN THERMOELECTRIC ELASTICITY THEORY, the piezoelectric effect on the thermoelastic Lamb wave propagation in the functionally graded material (FGM) plate is investigated. The coupled wave equations are solved by employing the Legendre polynomial series approach (LSPA), which poses the advantages of small scale of eigenvalues matrix and a convenient solution. It can directly obtain the complex wave number solutions without iteration. The obtained complex solutions, which represent the wave propagation and attenuation, are compared with those available data. Numerical examples show that the influence of gradient is profound. Results indicate that the piezoelectric effects on attenuation with the open and closed circuit condition are consistent for the S0 and S1 modes, but are inconsistent for the A0 and A1 modes. Although the piezoelectric effect is weak on the dispersion and attenuation of thermal waves, it is notable for their physical field distributions. In addition, the relaxation time is critical to electric displacements of a thermal wave mode, but is not essential for those of Lamb-like modes. The results can be used for the optimization of thermo-electric-elastic coupling structures.

Key words: thermoelastic wave, attenuation, FGM, piezoelectric effect, physical field distributions.



Copyright © 2023 The Authors.

Published by IPPT PAN. This is an open access article under the Creative Commons Attribution License CC BY 4.0 (<https://creativecommons.org/licenses/by/4.0/>).

1. Introduction

FUNCTIONAL GRADED PIEZOELECTRIC MATERIALS (FGPM) (BRISCHETTO and CARRERA [1], SU *et al.* [2], AREFI *et al.* [3]) are a typical representative of the Functional-Intelligent integrated advanced composites. Through the appropriate combination of different materials, unique piezoelectric materials that meet various needs and change in the desired direction of electroelastic properties can be manufactured. As the advantages in intelligent control, damage detection and signal transmission, play an important role in the field of structural health monitoring (PAL and SINGH [4]) and electromechanical system (GUO *et al.* [5]).

The research on the FGPM has involved various aspects of its mechanical properties, such as vibration (KUMAR and HARSHA [6], LU *et al.* [7]), bending (HE *et al.* [8], SATOR *et al.* [9]), bulking (ANSARI *et al.* [10], TORABI *et al.* [11]),

nonlinearity (KOMIJANI *et al.* [12], ZHOU *et al.* [13]), wave motions (NOROUZ-ZADEH *et al.* [14], GUO *et al.* [15], EZZIN *et al.* [16]), etc. The wave characteristics of FGPM structures are related directly to their performances in transducers, resonators and vibration filters, and have attracted a lot of attention. CHAKI and SINGH [17] investigated the propagation characteristics of SH surface waves in irregular imperfectly-bonded layered FGPM. Basing on the axisymmetric isogeometric analysis, LI and HAN [18] studied the dispersion properties of wave propagation in a sandwich structure composed of FG nanocomposite core and piezoelectric surface layers. ZHANG *et al.* [19, 20] considered the guided wave characteristics in FG hexagonal piezoelectric quasi-crystal cylinders and in FGP cylindrical shells. EZZIN *et al.* [21] analyzed the response in FG magneto-electro-elastic plates. HEYDARPOUR *et al.* [22] considered a thermoelastic response in FG cylindrical panels with piezoelectric layers. SAROJ *et al.* [23] discussed the Love-type surface waves characteristics in composite structures with initial stress. LI *et al.* [24] investigated the thickness-twist waves in FGPM. SHARMA and KUMAR [25] studied the Love-type wave in a layered structure consisting of the FGPM stratum followed by a semi-infinite couple-stress substrate exhibiting microstructural properties. XUE and PAN [26] discussed the longitudinal wave in FG magneto-electro-elastic rod. MOHAMMADI [27] analyzed the electro-elastic response of the porous cored-sandwich cylindrical pressure vessels with piezoelectric face-sheets, immersed in the Pasternak foundation.

The FGPM usually works in the multi-physical fields' environment, including force field, electric field, temperature field, etc. Therefore, the influence of temperature has to be considered in its wave analysis. To the author's knowledge, there are no relevant reports on thermoelastic wave propagation in FGPM structures, although it is an important research aspect in the field of wave mechanics. Even now lacking of research on a guided wave in thermo-electric-elastic coupling structures, the relevant available research can provide a basis. The results on a pure elastic wave in FGPM indicate that the piezoelectric effect has a significant influence on the dispersion curves, displacement and stress distributions, but does not add new modes (YU *et al.* [28]). Meanwhile, the results in the functional graded materials (FGM) plates (WANG *et al.* [29]) showed that the thermoelastic coupling produces thermal wave modes. Importantly, thermoelasticity leads to a non-ignorable attenuation on the elastic waves. SHARMA and PAL [30] discussed the influences of insulated and isothermal boundary conditions, as well as the propagation direction on Lamb-like waves in a piezoelectric plate with the thermal effect, and results showed that the attenuation is remarkable. With above discussions, intense interest is aroused on the study of the piezoelectric effect on thermoelastic wave in the FGPM plate, especially on its attenuation, as that the attenuation directly affects the structural performance.

In this paper, the piezoelectric effect on the thermoelastic Lamb wave in FGPM plates is investigated based on the Lord–Shulman (LS) thermoelectric elasticity theory (SHARMA and PAL [30]). The Legendre polynomial series approach (LPSA) is extended to solve the coupled thermo-electric-elastic wave equations. It can transform the coupled wave equations into linear eigenvalue problems. Thus, the complex eigenvalues representing the propagation and attenuation of guided waves can be obtained directly. The LPSA has advantages of small matrix scale and convenient solution, and is widely used in wave propagation and vibration fields (LIU *et al.* [31], OTHMANI *et al.* [32], ZHENG *et al.* [33]). A comparative study and the convergence analysis show the validity of the LPSA. In this paper, the piezoelectric effect on phase velocity, attenuation and physical field distributions are discussed for FGMP plates with different electrical boundary conditions, and with different material distributions. Results reveal some new wave characteristics, which are of great significance in designing the thermo-electric-elastic coupling structures.

2. Mathematical model and solving process

2.1. Mathematical model

The geometry of a FGPM plate composed of two piezoelectric materials is shown in Fig. 1. Its thickness is h . The guided waves propagate in the x -direction. Based on the LS theory (SHARMA and PAL [30]), the basic equations are listed as follows:

$$(2.1a) \quad \sigma_{ij,j} = \rho \ddot{u}_i,$$

$$(2.1b) \quad D_{j,j} = 0,$$

$$(2.1c) \quad K_j T_{,jj} - \rho C_e (\dot{T} + t_0 \ddot{T}) = T_0 \beta_j (\dot{\epsilon}_{jj} + t_0 \ddot{\epsilon}_{jj}) - T_0 P_3 (\dot{\Phi}_{,z} + t_0 \ddot{\Phi}_{,z}).$$

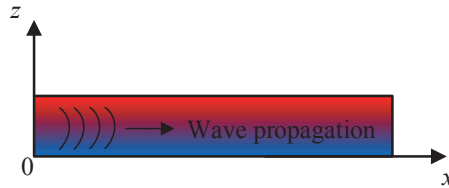


FIG. 1. A FGPM plate in Cartesian coordinate system.

Constitutive relations and geometric relations are:

$$(2.2a) \quad \sigma_{ij} = C_{ijkl} \varepsilon_{kl} - \beta_j T - e_{jk} E_k,$$

$$(2.2b) \quad D_j = e_{jkl} \varepsilon_{kl} + \epsilon_{jk} E_k + P_j T,$$

$$(2.2c) \quad \varepsilon_{jk} = \frac{1}{2}(u_{j,k} + u_{k,j}),$$

$$(2.2d) \quad E_j = -\Phi_{,j},$$

where σ_{ij} , ε_{ij} and u_j are the components of the stress, strain and displacement, respectively. D_i indicates the electric displacement components. C_{is} , e_{is} and ϵ_{is} are the components of the elastic stiffness, piezoelectric constant and dielectric constant, respectively. P_j is the pyroelectric constant; Φ is the electric potential; ρ is the material density; t and t_0 indicate the time and relaxation time; β_j and C_e are the volume expanding coefficients and specific heat at constant strain, respectively; K_j is the material constant characteristics; T and T_0 are the temperature variation and reference temperature, respectively; E_j is the electric field intensity.

Considering the stress-free boundary condition, the z -direction stress components should be zero as

$$(2.3) \quad \sigma_{jz}|_{z=0,h} = 0.$$

The adiabatic boundary condition is

$$(2.4) \quad T_{,z}|_{z=0,h} = 0.$$

The electrical open circuit and closed circuit conditions are considered in this paper, that is:

$$(2.5a) \quad \Phi|_{z=0,h} = 0 \quad \text{closed circuit,}$$

$$(2.5b) \quad D_z|_{z=0,h} = 0 \quad \text{open circuit.}$$

For the convenience of solution, the dimensionlessness is given:

$$(2.6) \quad \begin{aligned} \eta &= \frac{(\bar{\beta}_1)^2 T_0}{\bar{\rho}^2 \bar{C}_e v_x^2}, & \hat{x}_i &= \frac{v_x}{k_x} x_i, & \hat{u}_i &= \frac{v_x^3 \bar{\rho}}{k_x \bar{\beta}_1 T_0} u_i, & \tau_0 &= \frac{v_x^2}{k_x} t_0, \\ \hat{T} &= \frac{T}{T_0}, & \hat{T}_{ij} &= \frac{1}{\bar{\beta}_1 T_0} \sigma_{ij}, & \hat{\Phi} &= \frac{v_x \bar{e}_{33}}{k_x \bar{\beta}_1 T_0} \Phi, & \hat{D}_i &= \frac{\bar{C}_{11}}{\bar{\beta}_1 T_0 \bar{e}_{33}} D_i, \\ \hat{P}_i &= \frac{P_i \bar{C}_{11}}{\bar{\beta}_1 \bar{e}_{33}}, & \hat{\epsilon}_{ij} &= \frac{\epsilon_{ij} \bar{C}_{11}}{(\bar{e}_{33})^2}, & \hat{C}_{ij} &= \frac{C_{ij}}{\bar{C}_{11}}, & \hat{\beta}_i &= \frac{\beta_i}{\bar{\beta}_1}, \\ \hat{e}_{ij} &= \frac{e_{ij}}{\bar{e}_{33}}, & \hat{K}_i &= \frac{K_i}{\bar{K}_1}, & \hat{\rho} &= \frac{\rho}{\bar{\rho}}, & \hat{C}_e &= \frac{C_e}{\bar{C}_e}, \end{aligned}$$

where $v_x = \sqrt{\bar{C}_{11}/\bar{\rho}}$ is the longitudinal wave velocity, $k_x = \bar{K}_1/\bar{\rho}\bar{C}_e$ being the thermal diffusivity in the x direction; τ_0 is the dimensionless relaxation time.

2.2. Solution for electrical open circuit condition

Considering the dimensionless Eq. (2.6), and rewriting $\hat{\bullet}$ to \bullet for simplicity, the electric-elastic boundary conditions can be expressed as:

$$(2.7a) \quad T_{zz} = \left(C_{13} \frac{\partial u_x}{\partial x} + C_{23} \frac{\partial u_y}{\partial y} + C_{33} \frac{\partial u_z}{\partial z} - \beta_3 T + e_{33} \frac{\partial \Phi}{\partial \hat{z}} \right) \pi_{0,h}(z),$$

$$(2.7b) \quad T_{yz} = \left(C_{44} \frac{\partial u_y}{\partial z} + C_{44} \frac{\partial u_z}{\partial y} + e_{24} \frac{\partial \Phi}{\partial y} \right) \pi_{0,h}(z),$$

$$(2.7c) \quad T_{xz} = \left(C_{55} \frac{\partial u_x}{\partial z} + C_{55} \frac{\partial u_z}{\partial x} + e_{15} \frac{\partial \Phi}{\partial x} \right) \pi_{0,h}(z),$$

$$(2.7d) \quad D_z = \left(e_{31} \frac{\partial u_x}{\partial x} + e_{32} \frac{\partial u_y}{\partial y} + e_{33} \frac{\partial u_z}{\partial z} - \epsilon_{33} \frac{\partial \Phi}{\partial z} + P_3 T \right) \pi_{0,h}(z),$$

$\pi_{0,h}(\hat{z})$ is the rectangular window function,

$$(2.8) \quad \pi(z) = \begin{cases} 1, & 0 \leq z \leq h, \\ 0, & \text{else.} \end{cases}$$

The effectiveness of rectangular window function in dealing with boundary conditions has been proved (LEFEBVRE *et al.* [34]). In addition, the adiabatic boundary condition is expressed by the orthogonal polynomial series of temperature later.

Substituting Eqs. (2.2)–(2.7) into Eq. (2.1),

$$(2.9a) \quad C_{11} \frac{\partial^2 u_x}{\partial x^2} + C_{12} \frac{\partial^2 u_y}{\partial x \partial y} + C_{13} \frac{\partial^2 u_z}{\partial x \partial z} - \beta_1 \frac{\partial T}{\partial x} + e_{31} \frac{\partial^2 \Phi}{\partial x \partial z} + C_{66} \frac{\partial^2 u_x}{\partial y^2} \\ + C_{66} \frac{\partial^2 u_y}{\partial x \partial y} + \frac{\partial}{\partial \hat{z}} (C_{55}) \frac{\partial u_x}{\partial z} + C_{55} \frac{\partial^2 u_x}{\partial z^2} + \frac{\partial}{\partial z} (C_{55}) \frac{\partial u_z}{\partial x} \\ + C_{55} \frac{\partial^2 u_z}{\partial x \partial z} + \frac{\partial}{\partial z} (e_{15}) \frac{\partial \Phi}{\partial x} + e_{15} \frac{\partial^2 \Phi}{\partial x \partial z} \\ + \left(C_{55} \frac{\partial u_x}{\partial z} + C_{55} \frac{\partial u_z}{\partial x} + e_{15} \frac{\partial \Phi}{\partial x} \right) \frac{\partial \pi(z)}{\partial z} = \rho \frac{\partial^2 u_x}{\partial t^2},$$

$$(2.9b) \quad C_{66} \frac{\partial^2 u_x}{\partial x \partial y} + C_{66} \frac{\partial^2 u_y}{\partial x^2} + C_{12} \frac{\partial^2 u_x}{\partial x \partial y} + C_{22} \frac{\partial^2 u_y}{\partial y^2} + C_{23} \frac{\partial^2 u_z}{\partial y \partial z} - \beta_2 \frac{\partial T}{\partial y} \\ + e_{32} \frac{\partial^2 \Phi}{\partial y \partial z} + \frac{\partial}{\partial z} (C_{44}) \frac{\partial u_y}{\partial z} + C_{44} \frac{\partial^2 u_y}{\partial z^2} + \frac{\partial}{\partial z} (C_{44}) \frac{\partial u_z}{\partial y} \\ + C_{44} \frac{\partial^2 u_z}{\partial y \partial z} + \frac{\partial}{\partial z} (e_{24}) \frac{\partial \Phi}{\partial y} + e_{24} \frac{\partial^2 \Phi}{\partial y \partial z} \\ + \left(C_{44} \frac{\partial u_y}{\partial z} + C_{44} \frac{\partial u_z}{\partial y} + e_{24} \frac{\partial \Phi}{\partial y} \right) \frac{\partial \pi(z)}{\partial z} = \rho \frac{\partial^2 u_y}{\partial t^2},$$

$$\begin{aligned}
(2.9c) \quad & C_{55} \frac{\partial^2 u_x}{\partial x \partial z} + C_{55} \frac{\partial^2 u_z}{\partial x^2} + e_{15} \frac{\partial^2 \Phi}{\partial x^2} + C_{44} \frac{\partial^2 u_y}{\partial y \partial z} + C_{44} \frac{\partial^2 u_z}{\partial y^2} + e_{24} \frac{\partial^2 \Phi}{\partial y^2} \\
& + \frac{\partial}{\partial z} (C_{13}) \frac{\partial u_x}{\partial x} + C_{13} \frac{\partial^2 u_x}{\partial x \partial z} + \frac{\partial}{\partial z} (C_{23}) \frac{\partial u_y}{\partial y} + C_{23} \frac{\partial^2 u_y}{\partial y \partial z} \\
& + \frac{\partial}{\partial z} (C_{33}) \frac{\partial u_z}{\partial z} + C_{33} \frac{\partial^2 u_z}{\partial z^2} - \frac{\partial}{\partial z} (\beta_3) T - \beta_3 \frac{\partial T}{\partial z} \\
& + \frac{\partial}{\partial z} (e_{33}) \frac{\partial \Phi}{\partial z} + e_{33} \frac{\partial^2 \Phi}{\partial z^2} \\
& + \left(C_{13} \frac{\partial u_x}{\partial x} + C_{23} \frac{\partial u_y}{\partial y} + C_{33} \frac{\partial u_z}{\partial z} - \beta_3 T + e_{33} \frac{\partial \Phi}{\partial z} \right) \frac{\partial \pi(z)}{\partial z} \\
& = \rho \frac{\partial^2 u_z}{\partial t^2},
\end{aligned}$$

$$\begin{aligned}
(2.9d) \quad & K_1 \frac{\partial^2 T}{\partial x^2} + K_2 \frac{\partial^2 T}{\partial y^2} + \hat{K}_3 \frac{\partial^2 T}{\partial z^2} - \beta_1 \eta \left(1 + \tau_0 \frac{\partial}{\partial t} \right) \frac{\partial}{\partial t} \frac{\partial u_x}{\partial x} \\
& - \beta_2 \eta \left(1 + \tau_0 \frac{\partial}{\partial t} \right) \frac{\partial}{\partial t} \frac{\partial u_y}{\partial y} - \beta_3 \eta \left(1 + \tau_0 \frac{\partial}{\partial t} \right) \frac{\partial}{\partial t} \frac{\partial u_z}{\partial z} \\
& + P_3 \eta \left(1 + \tau_0 \frac{\partial}{\partial t} \right) \frac{\partial \Phi}{\partial t \partial z} = \rho C_e \left(1 + \tau_0 \frac{\partial}{\partial t} \right) \frac{\partial T}{\partial t},
\end{aligned}$$

$$\begin{aligned}
(2.9e) \quad & e_{15} \frac{\partial^2 u_x}{\partial x \partial z} + e_{15} \frac{\partial^2 u_z}{\partial x^2} - \epsilon_{11} \frac{\partial^2 \Phi}{\partial x^2} + P_1 \frac{\partial T}{\partial x} + e_{24} \left(\frac{\partial^2 u_y}{\partial y \partial z} + \frac{\partial^2 u_z}{\partial y^2} \right) \\
& - \epsilon_{22} \frac{\partial^2 \Phi}{\partial y^2} + P_2 \frac{\partial T}{\partial y} + \frac{\partial}{\partial z} (e_{31}) \frac{\partial u_x}{\partial x} + e_{31} \frac{\partial^2 u_x}{\partial x \partial z} \\
& + \frac{\partial}{\partial z} (e_{32}) \frac{\partial u_y}{\partial y} + e_{32} \frac{\partial^2 u_y}{\partial y \partial z} + \frac{\partial}{\partial z} (e_{33}) \frac{\partial u_z}{\partial z} \\
& + e_{33} \frac{\partial^2 u_z}{\partial z^2} - \frac{\partial}{\partial z} (\epsilon_{33}) \frac{\partial \Phi}{\partial z} - \epsilon_{33} \frac{\partial^2 \Phi}{\partial z^2} \frac{\partial}{\partial z} (P_3) T + P_3 \frac{\partial T}{\partial z} \\
& + \left(\frac{e_{31}}{\bar{e}_{33} \frac{\partial u_x}{\partial x}} + e_{32} \frac{\partial u_y}{\partial y} + e_{33} \frac{\partial u_z}{\partial z} - \epsilon_{33} \frac{\partial \Phi}{\partial z} + P_3 T \right) \frac{\partial \pi(z)}{\partial z} = 0.
\end{aligned}$$

Since the wave propagates in the x direction, the displacements, electric potential and temperature variables can be assumed as:

$$(2.10a) \quad u_x(x, y, z, t) = \exp(ikx - i\omega t)U(z),$$

$$(2.10b) \quad u_y(x, y, z, t) = \exp(ikx - i\omega t)V(z),$$

$$(2.10c) \quad u_z(x, y, z, t) = \exp(ikx - i\omega t)W(z),$$

$$(2.10d) \quad T(x, y, z, t) = \exp(ikx - i\omega t)X(z),$$

$$(2.10e) \quad \Phi(x, y, z, t) = \exp(ikx - i\omega t)Y(z).$$

Among them, $U(z)$, $V(z)$, $W(z)$ are the displacement amplitudes in the x , y , and z directions, respectively. $X(z)$ and $Y(z)$ are the temperature amplitude and the

electric potential amplitude in the z direction, respectively; k is the wave number, and $k = \text{Re}(k) + i \cdot \text{Im}(k)$. The real part of k represents the propagation of wave and the imaginary part represents the attenuation; ω is the angular frequency.

Similar as CAO *et al.* [35], all material properties in the FGM are expanded as follows:

$$\begin{aligned}
 \hat{C}_{ij}(z) &= C_{ij}^{(l)} \left(\frac{2z-h}{h} \right)^l, & \hat{\rho}_i(z) &= \rho_i^{(l)} \left(\frac{2z-h}{h} \right)^l, \\
 \hat{e}_{ij}(z) &= e_{ij}^{(l)} \left(\frac{2z-h}{h} \right)^l, & \hat{\epsilon}_{ij}(z) &= \epsilon_{ij}^{(l)} \left(\frac{2z-h}{h} \right)^l, \\
 \hat{K}_i(z) &= K_i^{(l)} \left(\frac{2z-h}{h} \right)^l, & \hat{\beta}_i(z) &= \beta_i^{(l)} \left(\frac{2z-h}{h} \right)^l, \\
 \hat{C}_e(z) &= C_e^{(l)} \left(\frac{2z-h}{h} \right)^l, & \hat{P}_i(z) &= P_i^{(l)} \left(\frac{2z-h}{h} \right)^l, \quad l = 1, \dots, L.
 \end{aligned}
 \tag{2.11}$$

On account of Eqs. (2.9)–(2.11), the following equations are obtained,

$$\begin{aligned}
 (2.12a) \quad & \sum_{l=0}^L \left(\frac{2z-h}{h} \right)^l \{ -k^2 C_{11}^{(l)} U + ik(C_{13}^{(l)} + C_{55}^{(l)})W' - ik\beta_1^{(l)} X \\
 & + ik(e_{31}^{(l)} + e_{15}^{(l)})Y' + C_{55}^{(l)} U'' + (C_{55}^{(l)} U' + ikC_{55}^{(l)} W + ik e_{15}^{(l)} Y) \pi'_{0,h}(z) \} \\
 & + \frac{2}{h} \sum_{n=1}^L \left(\frac{2z-h}{h} \right)^{l-1} (C_{55}^{(l)} U' + ikC_{55}^{(l)} W + ik e_{15}^{(l)} Y) = -\omega^2 \sum_{n=0}^L \rho^{(l)} \left(\frac{2z-h}{h} \right)^l U,
 \end{aligned}$$

$$\begin{aligned}
 (2.12b) \quad & \sum_{l=0}^L \left(\frac{2z-h}{h} \right)^l [-k^2 C_{66}^{(l)} V + C_{44}^{(l)} (V'' + V' \pi'_{0,h}(z))] \\
 & + \frac{2}{h} \sum_{l=1}^L \left(\frac{2z-h}{h} \right)^{l-1} C_{44}^{(l)} V' \pi_{0,h}(z) = -\omega^2 \sum_{l=0}^L \rho^{(l)} \left(\frac{2z-h}{h} \right)^l V,
 \end{aligned}$$

$$\begin{aligned}
 (2.12c) \quad & \sum_{l=0}^L \left(\frac{2z-h}{h} \right)^l \{ ikC_{55}^{(l)} U' - k^2 C_{55}^{(l)} W - k^2 e_{15}^{(l)} Y + ikC_{13}^{(l)} U' + C_{33}^{(l)} W'' \\
 & - \beta_3^{(l)} X' + e_{33}^{(l)} Y'' + (ikC_{13}^{(l)} U + C_{33}^{(l)} W' - \beta_3^{(l)} X + e_{33}^{(l)} Y') \pi'_{0,h}(z) \} \\
 & + \frac{2}{h} \sum_{l=1}^L \left(\frac{2z-h}{h} \right)^{l-1} (ikC_{13}^{(l)} U + C_{33}^{(l)} W' - \beta_3^{(l)} X + e_{33}^{(l)} Y') \\
 & = -\omega^2 \sum_{l=0}^L \rho^{(l)} \left(\frac{2z-h}{h} \right)^l W,
 \end{aligned}$$

$$\begin{aligned}
(2.12d) \quad & \sum_{l=0}^L \left(\frac{2z-h}{h} \right)^l \left[-k^2 K_1^{(l)} X + K_3^{(l)} X'' - (1-i\omega\tau_0)(k\omega\eta\beta_1^{(l)} U \right. \\
& \quad \left. - i\omega\eta\beta_3^{(l)} W' + i\omega\eta P_3^{(l)} Y') \right] \\
& = -i\omega \sum_{l=0}^L \sum_{m=0}^L \rho^{(l)} C_e^{(m)} \left(\frac{2z-h}{h} \right)^l \left(\frac{2z-h}{h} \right)^m (1-i\omega\tau_0) X,
\end{aligned}$$

$$\begin{aligned}
(2.12e) \quad & \sum_{l=0}^L \left(\frac{2z-h}{h} \right)^l \left\{ [(ike_{15}^{(l)} U' - k^2 e_{15}^{(l)} W) + ikP_1^{(l)} X + k^2 \epsilon_{11}^{(l)} Y] \right. \\
& \quad + (ike_{31}^{(l)} U' + e_{33}^{(l)} W'' - \epsilon_{33}^{(l)} Y'' + P_3^{(l)} X') \\
& \quad \left. + (ike_{31}^{(l)} U + e_{33}^{(l)} W' - \epsilon_{33}^{(l)} Y' + P_3^{(l)} X) \pi'_{0,h}(z) \right\} \\
& \quad + \frac{2}{h} \sum_{l=1}^L \left(\frac{2z-h}{h} \right)^{l-1} (ike_{31}^{(l)} U + e_{33}^{(l)} W' - \epsilon_{33}^{(l)} Y' + P_3^{(l)} X) = 0.
\end{aligned}$$

Equation (2.12b) is independent of the others, and represents the SH waves. The coupled wave Eqs. (2.12a, 2.12c–2.12e) express the thermo-electric-elastic Lamb waves. In this paper, the SH waves are not considered.

To obtain the characteristics of thermo-electric-elastic Lamb waves, physical field amplitudes are approximated by Legendre polynomials series:

$$\begin{aligned}
(2.13) \quad & U(z) = \sum_{n=0}^{\infty} p_n^{(1)} Q_n(z), \quad W(z) = \sum_{n=0}^{\infty} p_n^{(2)} Q_n(z), \\
& X(z) = \sum_{n=0}^{\infty} p_n^{(3)} Q_n(z), \quad Y(z) = \sum_{n=0}^{\infty} p_n^{(4)} Q_n(z),
\end{aligned}$$

where

$$(2.14) \quad Q_n(z) = \sqrt{\frac{2n+1}{h}} P_n \left(\frac{2z-h}{h} \right).$$

With the increase of the expanded order n , the influence of higher-order terms of polynomials on the overall results decreases rapidly. As a result, the summation over Eq. (2.13) should be halted at some value N .

The adiabatic boundary condition can be expressed by a new Legendre polynomials series,

$$(2.15) \quad X'(z) = \pi(z) \sum_{n=0}^N P_n^5 \frac{d}{dz} Q_n(z).$$

The derivative of $X(z)$ must equal to $X'(z)$ (that is, the temperature gradient expression). Multiplying both sides of Eq. (2.12) by $Q_j(z)$, $j = 0, 1, \dots, N$, and integrating from 0 to \bar{h} , the relationship of $p^{(3)}$ and $p^{(5)}$ can be obtained as:

$$(2.16) \quad Hp^{(3)} = Hp^{(5)} \Rightarrow p^{(3)} = p^{(5)}.$$

Therefore, although the expansion of the temperature gradient is given, the total number of variables does not increase.

Similarly as in the process of Eq. (2.16), we have the following matrix equations:

$$(2.17) \quad k^2 Ap + kBp + Cp = Mp,$$

here:

$$A = \begin{bmatrix} A_{11} & 0 & 0 & 0 \\ 0 & A_{22} & 0 & A_{24} \\ 0 & 0 & A_{33} & 0 \\ 0 & A_{42} & 0 & A_{44} \end{bmatrix}, \quad B = \begin{bmatrix} 0 & B_{12} & B_{13} & B_{14} \\ B_{21} & 0 & 0 & 0 \\ B_{31} & 0 & 0 & 0 \\ B_{41} & 0 & B_{43} & 0 \end{bmatrix},$$

$$C = \begin{bmatrix} C_{11} & 0 & 0 & 0 \\ 0 & C_{22} & C_{23} & C_{24} \\ 0 & C_{32} & C_{33} & C_{34} \\ 0 & C_{42} & C_{43} & C_{44} \end{bmatrix}, \quad M = \begin{bmatrix} M_{11} & 0 & 0 & 0 \\ 0 & M_{11} & 0 & 0 \\ 0 & 0 & M_{33} & 0 \\ 0 & 0 & 0 & 0 \end{bmatrix},$$

$$p = \begin{bmatrix} p_n^{(1)} & p_n^{(2)} & p_n^{(3)} & p_n^{(4)} \end{bmatrix}^T.$$

The dimension of matrices A_{ij} , B_{ij} , C_{ij} , M_{ij} are $(N + 1) \times (N + 1)$, and their detailed expressions can be found in Appendix A.

In order to reduce the solving difficulty, the quadratic eigenvalue problem (2.17) is further transformed into a linear eigenvalue problem by using a new wavenumber dependent vector

$$(2.18) \quad q = kp,$$

and the final characteristic equation is obtained,

$$(2.19) \quad \begin{bmatrix} 0 & I \\ A^{-1}(M - C) & -A^{-1}B \end{bmatrix} \begin{bmatrix} p \\ q \end{bmatrix} = k \begin{bmatrix} p \\ q \end{bmatrix}.$$

Basing on Eq. (2.19), the dispersion curves and physical field distributions can be solved quickly.

2.3. Solution for electrical closed circuit condition

The electrically closed circuit boundary conditions limit the electric potential being zero at boundaries. The following changes can be made:

$$(2.20) \quad \Phi(x, y, z, t) = z(z - h) \exp(ikx - i\omega t)Y(z).$$

The rectangular window function for D_z is removed from Eq. (2.7).

Replacing the corresponding expression in Eq. (2.10e) by Eq. (2.20), and remaining others unchanged, the coupled wave equations are:

$$(2.21a) \quad \sum_{n=0}^L \left(\frac{2z-h}{h} \right)^n \left\{ -k^2 C_{11}^{(n)} U + ik(C_{13}^{(n)} + C_{55}^{(n)})W' - ik\beta_1^{(n)} X \right. \\ \left. + ike_{31}^{(n)} [z(z-h)Y]' + C_{55}^{(n)} U'' + ike_{15}^{(n)} [z(z-h)Y]' \right. \\ \left. + (C_{55}^{(n)} U' + ikC_{55}^{(n)} W + ike_{15}^{(n)} Y)\pi'_{0,h}(z) \right\} \\ + \frac{2}{h} \sum_{n=1}^L \left(\frac{2z-h}{h} \right)^{n-1} (C_{55}^{(n)} U' + ikC_{55}^{(n)} W + ike_{15}^{(n)} [z(z-h)Y]) \\ = -\omega^2 \sum_{n=0}^L \rho^{(n)} \left(\frac{2z-h}{h} \right)^n U,$$

$$(2.21b) \quad \sum_{n=0}^L \left(\frac{2z-h}{h} \right)^n \left\{ (ik(C_{55}^{(n)} + C_{13}^{(n)})U' - k^2 C_{55}^{(n)} W - k^2 e_{15}^{(n)} [z(z-h)Y] \right. \\ \left. + C_{33}^{(n)} W'' - \beta_3^{(n)} X' + e_{33}^{(n)} [z(z-h)Y]') \right. \\ \left. \times \sum_{n=0}^L \left(\frac{2z-h}{h} \right)^n (ikC_{13}^{(n)} U + C_{33}^{(n)} W' - \beta_3^{(n)} X + e_{33}^{(n)} [z(z-h)Y]')\pi'_{0,h}(z) \right\} \\ + \frac{2}{h} \sum_{n=1}^L \left(\frac{2z-h}{h} \right)^{n-1} (ikC_{13}^{(n)} U + C_{33}^{(n)} W' - \beta_3^{(n)} X + e_{33}^{(n)} [z(z-h)Y]') \\ = -\omega^2 \sum_{n=0}^L \rho^{(n)} \left(\frac{2z-h}{h} \right)^n W,$$

$$(2.21c) \quad \sum_{n=0}^L \left(\frac{2z-h}{h} \right)^n \left\{ -k^2 K_1^{(n)} X + K_3^{(n)} X'' \right. \\ \left. - (1 - i\omega\tau_0)(k\omega\eta\beta_1^{(n)} U - i\omega\eta\beta_3^{(n)} W' + i\omega\eta P_3^{(n)} [z(z-h)Y]') \right\} \\ = -i\omega \sum_{n=0}^L \sum_{m=0}^L \rho^{(n)} C_e^{(m)} \left(\frac{2z-h}{h} \right)^n \left(\frac{2z-h}{h} \right)^m (1 - i\omega\tau_0) X,$$

$$\begin{aligned}
(2.21d) \quad & \sum_{n=0}^L \left(\frac{2z-h}{h} \right)^n \left[ik(e_{15}^{(n)} + e_{31}^{(n)})U' - k^2 e_{15}^{(n)}W + ikP_1^{(n)}X \right. \\
& + k^2 \epsilon_1^{(n)} z(z-h)Y + e_{33}^{(n)}W'' - \epsilon_3^{(n)} [z(z-h)Y]'' + P_3^{(n)}X' \Big] \\
& + \frac{2}{h} \sum_{n=1}^L \left(\frac{2z-h}{h} \right)^{n-1} (ike_{31}^{(n)}U + e_{33}^{(n)}W' - \epsilon_3^{(n)} [z(z-h)Y]' + P_3^{(n)}X) = 0.
\end{aligned}$$

It is noted that the main change of above formulas lies in the electric potential $Y(z)$. As in the case of Eqs. (2.13)–(2.19), the solution for the electrical closed circuit condition can be obtained. The expressions of sub-matrices can be found in Appendix B.

3. Numerical examples and analysis

3.1. Verification and convergence of the LPSA

In order to verify the effectiveness of the LPSA, comparisons with open results (AMOR *et al.* [36], AL-QAHTANI and DATTA [37]) are given in Fig. 2. As mentioned earlier, due to lacking of available results, the comparison on dispersion curves has to be reduced for an FGM plate in Fig. 2(a), and that on attenuation is reduced for an uniform thermoelastic plate in Fig. 2(b). The consistent results indicate that the validity of the presented LPSA.

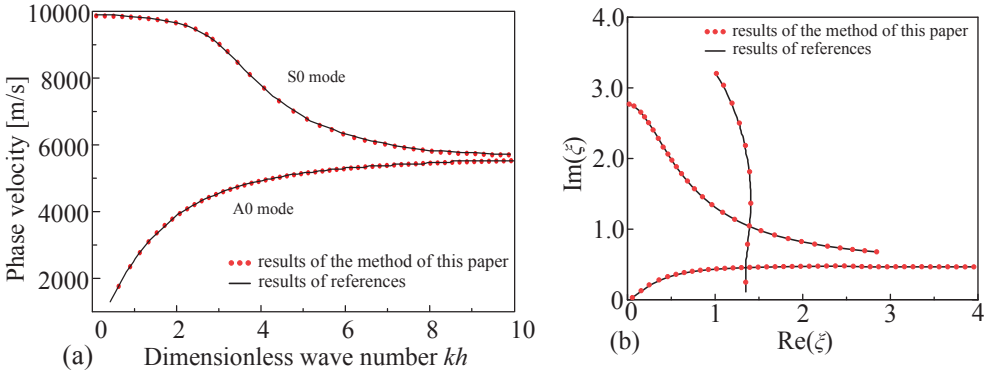


FIG. 2. Comparison with open results; (a) phase velocity [36], (b) imaginary parts [37]; kh – indicates the product of the wave number and thickness.

The convergence of the LPSA is exhibited in Figs. 3 and 4. It is clear that the first three dispersion curves are exactly consistent in Fig. 3(a) when $N = 6$ and 7. And, more mode curves agree with each other with increasing N , which is clear in Fig. 3(b). A similar situation can be found on attenuation curves in Fig. 4, which indicates that the first three modes are convergent with $N = 6$. This example

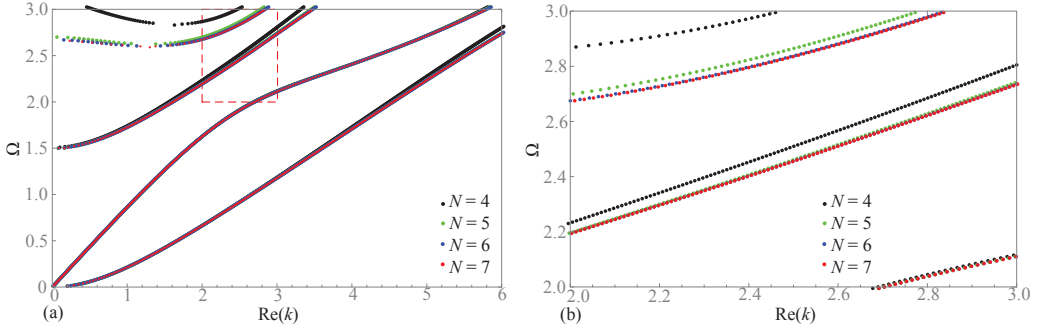


FIG. 3. Convergence analysis of dispersion curves, $L = 1$; (a) Lamb-like wave dispersion curves; (b) enlarged diagram of (a).

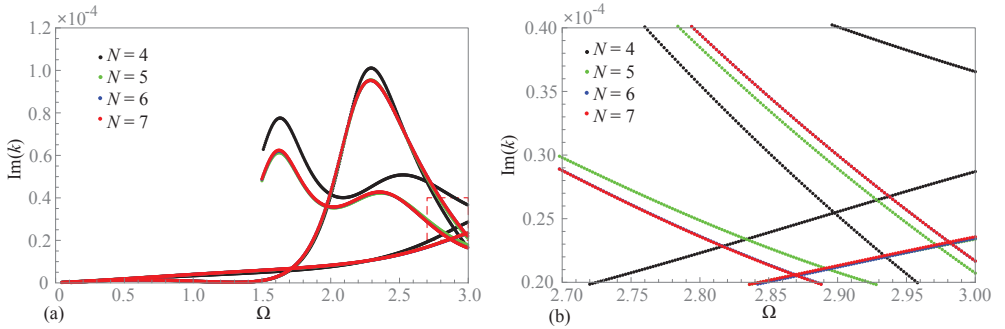


FIG. 4. Convergence analysis of attenuation curves, $L = 1$; (a) Lamb-like wave attenuation curves; (b) enlarged diagram of (a).

shows that the LSPA has order by order convergence. Rough judgment, the s -th mode should be analyzed with $2s$ order expansion of the Legendre polynomial. In this section, the first 4 modes are analyzed with $N = 8$.

3.2. Piezoelectric effect on wave propagation and attenuation

The piezoelectric effects on the Lamb-like wave and thermal wave are discussed in this section. The FGPM is composed of PZT-5A and CdSe. The material parameters (GUHA and SINGH [38]) are shown in Table 1. The functionally graded material parameters can be expressed as $P(z) = V_1 P_1(z) + V_2 P_2(z) P_i(z)$, V_i represents the volume fraction and the corresponding properties of upper and lower surfaces, respectively. In this paper, the material gradient is stated as $P_2(z) = (z/h)^L$ and $P_1(z) = 1 - (z/h)^L$. $L = 1, 2, \dots$

As shown in Figs. 5 and 6, the red and black curves are thermoelastic waves in the FGPM plates with the open and closed circuit conditions, respectively.

TABLE 1. The material properties [35].

Property	C_{11}	C_{12}	C_{13}	C_{33}	C_{44}	C_{55}	e_{31}	e_{33}	e_{15}
	[$10^9 \text{ N}\cdot\text{m}^{-2}$]						[$\text{C}\cdot\text{m}^{-2}$]		
CdSe	74.1	45.2	39.3	83.6	13.2	13.2	-0.16	0.347	-0.138
PZT-5A	139	77.8	75.4	113	25.6	25.6	-6.98	13.8	13.4
ε_{11}	ε_{33}	K_1	K_3	β_1	β_3	P_1	P_3	C_e	ρ
[$10^{-11} \text{ C}^2\cdot\text{N}^{-1}\cdot\text{m}^{-2}$]		[$\text{W}\cdot\text{m}^{-1}\cdot\text{K}^{-1}$]		[$10^6 \text{ N}\cdot\text{K}^{-1}\cdot\text{m}^{-2}$]		[$10^{-6} \text{ C}\cdot\text{K}^{-1}\cdot\text{m}^{-2}$]		[$\text{J}\cdot\text{kg}^{-1}\cdot\text{K}^{-1}$]	[$10^3 \text{ kg}\cdot\text{m}^{-3}$]
8.26	9.03	9	9	0.621	0.551	-2.94	-2.94	260	5.504
600	547	1.5	1.5	1.52	1.53	-452	-452	420	7.75

The blue ones are those in the FGM plate without electricity. Clearly, the phase velocity and attenuation curves of thermal waves are almost not affected by the piezoelectric effect in Fig. 5. Figure 6 depicts the phase velocity curves of

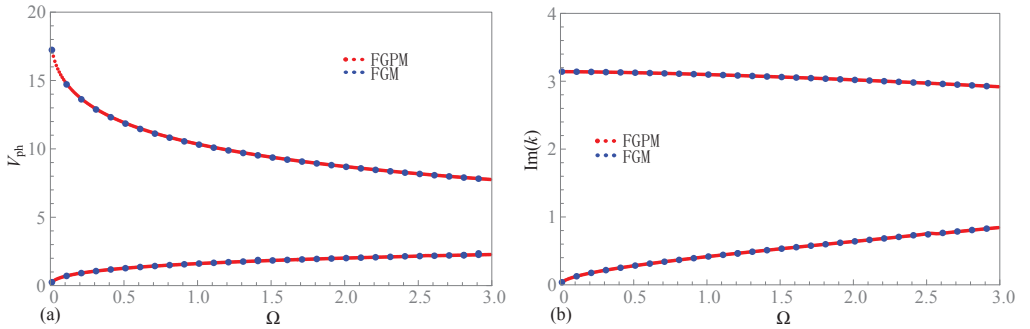


FIG. 5. Dispersion curves of thermal waves in the FGPM and FGM plates with $L = 1$; (a) phase velocity curves, (b) attenuation.

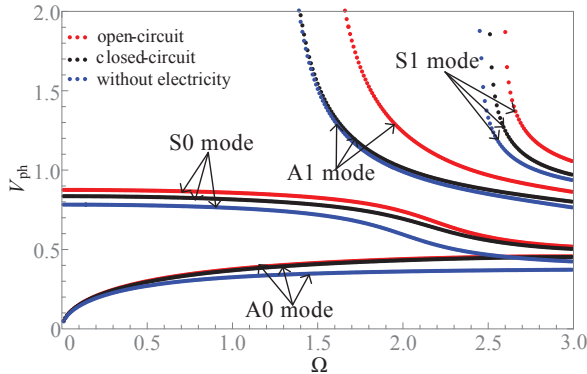


FIG. 6. Dispersion curves of Lamb-like waves in the FGM plate, $L = 1$.

Lamb-like waves. Results indicate that the piezoelectric effect increases the phase velocity, which is the same as that in [28]. The attenuation curves are shown in Fig. 7. Considering the closed circuit condition, (a) the piezoelectric effect enhances the attenuation of A0 mode, but decreases that of A1 modes; (b) the piezoelectric effect moves the minimal attenuation of S0 mode to a lower fre-

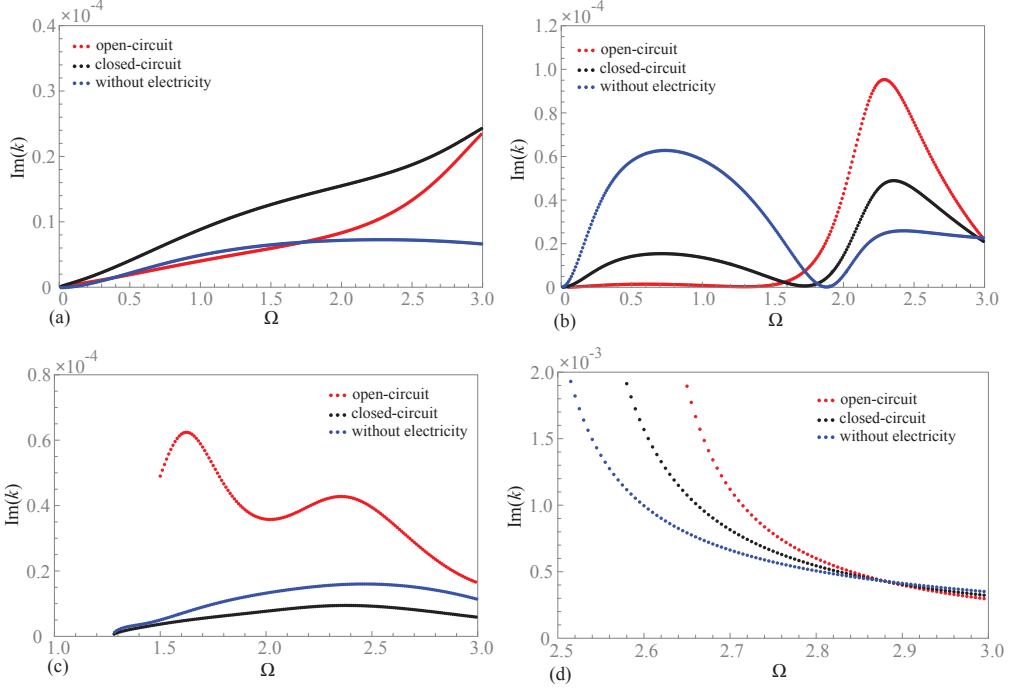


FIG. 7. Attenuation curves of Lamb-like waves in FGM plate; (a) A0 mode, (b) S0 mode, (c) A1 mode, (d) S1 mode.

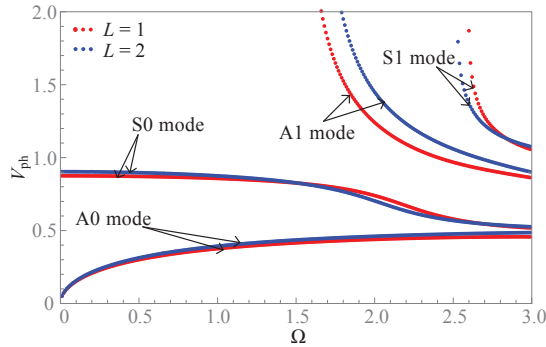


FIG. 8. Dispersion curves of Lamb-like waves in FGM plate with $L = 1$ and $L = 2$.

quency. Meanwhile, it has different influences on both sides of minimal attenuation; (c) there is a frequency at which the attenuation intensity changes for S0 and S1 modes. For the closed circuit condition, the cases (b) and (c) also occur. In addition, the piezoelectric effect raises the attenuation of A1 mode, but has

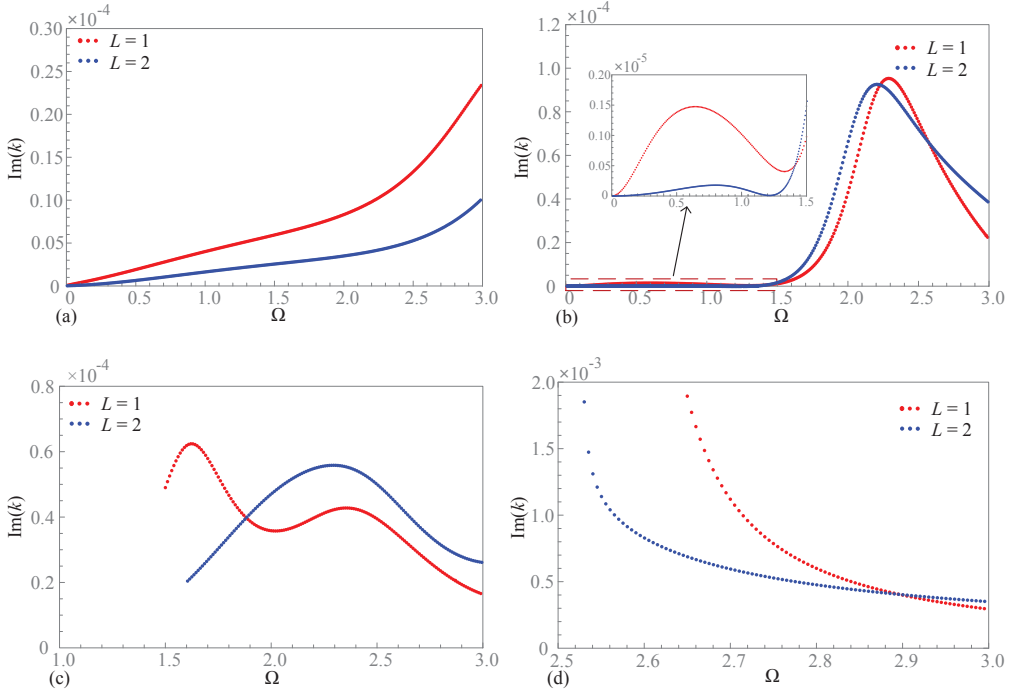


FIG. 9. Attenuation curves of Lamb-like waves in FGPM plate with $L = 1$ and $L = 2$; (a) A0 mode, (b) S0 mode, (c) A1 mode, (d) S1 mode.

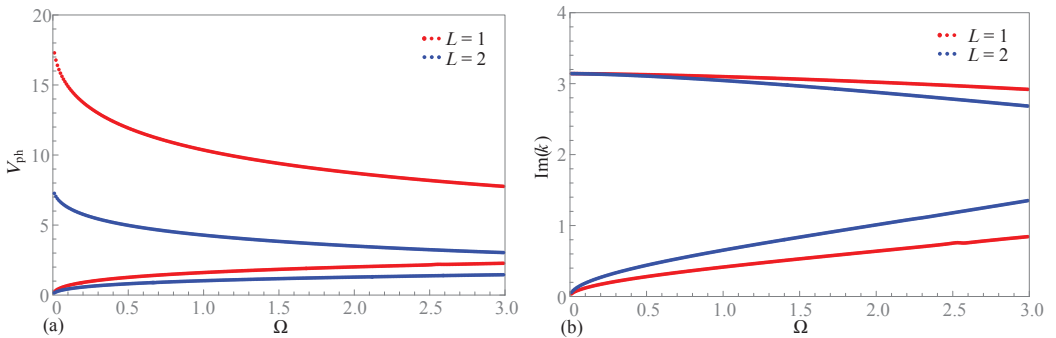


FIG. 10. Dispersion curves of thermal waves in FGPM plate with $L = 1$ and $L = 2$; (a) phase velocity curves, (b) attenuation curves.

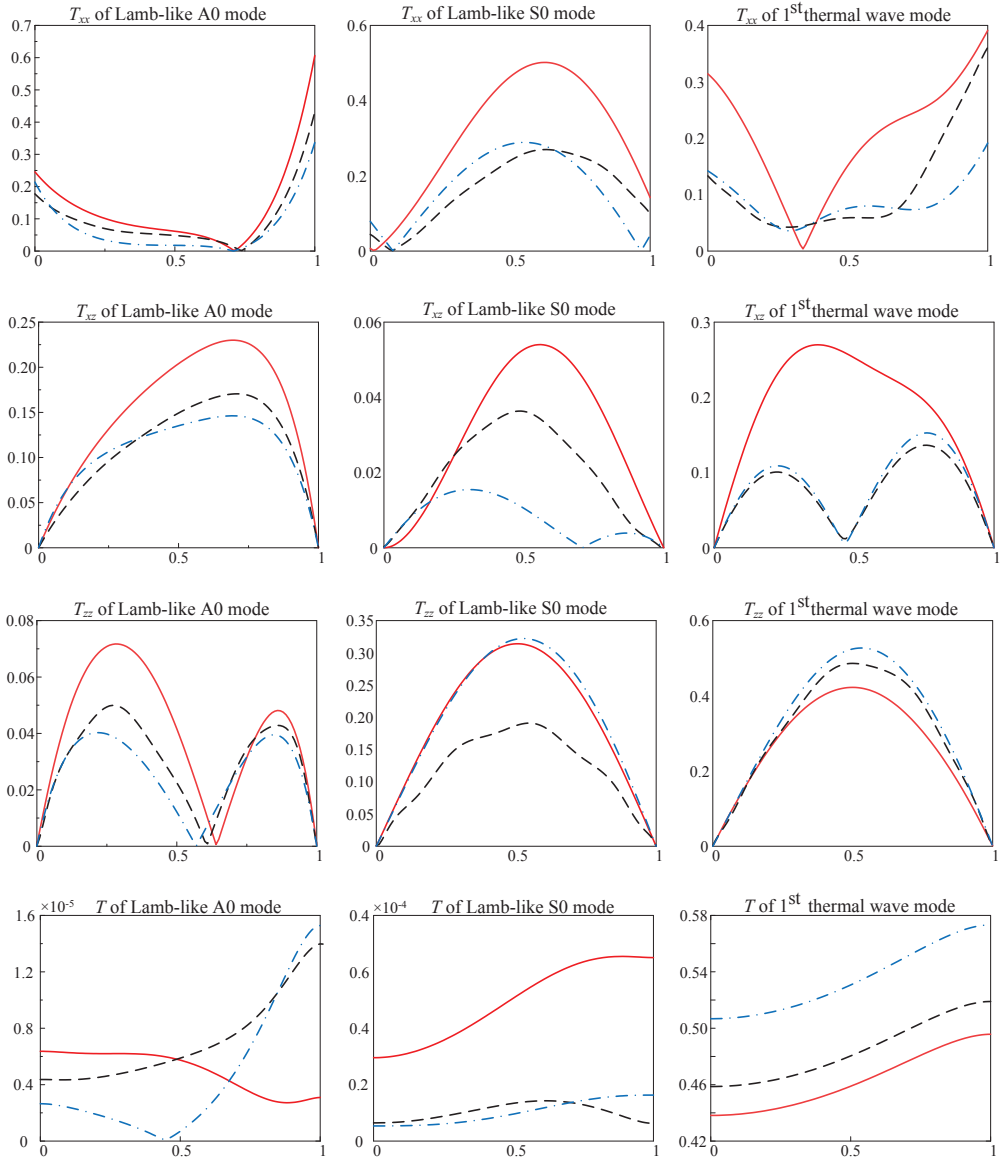


FIG. 11. Influence of piezoelectric effect, $\Omega = 2$; — electric open circuit, --- electric closed circuit, -.- without electricity.

no obvious trend on A0 mode. Overall, the piezoelectric effect is remarkable on attenuation.

Furthermore, the dispersion and attenuation curves in a different graded material are regarded in Figs. 8–10. The influence of gradient on phase velocities of

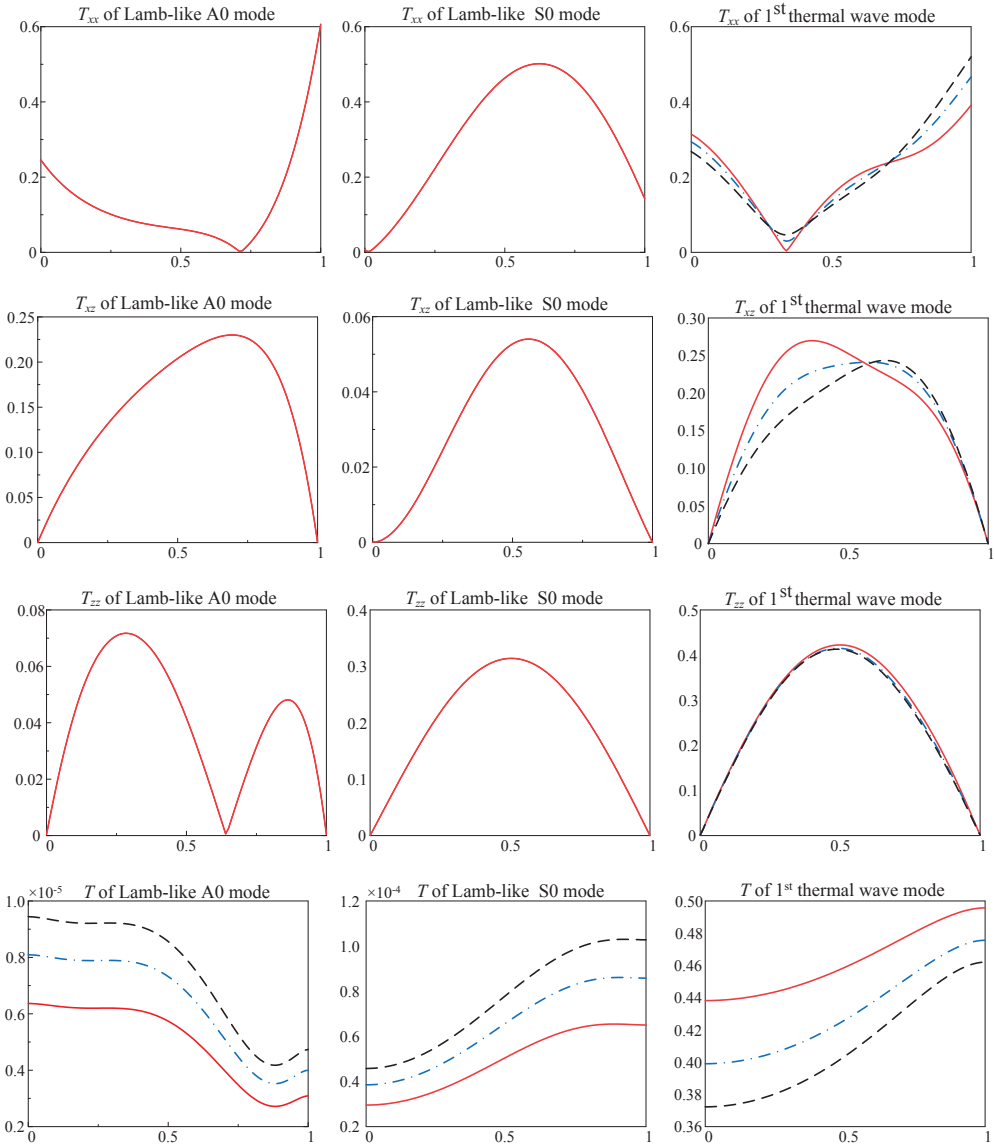


FIG. 12. Influence of relaxation time on stress and temperature, $\Omega = 2$;
 — $\tau_0 = 1$, --- $\tau_0 = 2$, -·-·- $\tau_0 = 3$.

higher modes is much larger than that on those of lower modes, either thermal waves or Lamb-like waves. Specifically, for antisymmetric modes A0 and A1, the phase velocities with $L = 2$ are larger than those with $L = 1$. But for symmetric modes S0 and S1, it should be considered in sections. Figure 9 shows the attenuation curves of the first four modes. Obviously, the attenuation trend of

the S0 and A0 modes has an almost opposite law with their dispersion. However, the attenuation of S1 and A1 modes has the same law with the dispersion for most frequencies. Besides, the attenuation with $L = 2$ is enhanced for the first thermal wave mode, and is suppressed for the second thermal wave mode in Fig. 10(b). Consequently, Figs. 8–10 show that the attenuation of fundamental modes (A0, S0 and the 1st thermal modes) is almost inconsistent with their dispersion curves, with $L = 1$ and 2, but that of higher modes (A1, S1 and the 2nd thermal modes) is consistent with their dispersion curves for most frequencies.

3.3. Piezoelectric effect on physical fields

The piezoelectric effect on displacements and temperature with $\Omega = 2$ is analyzed in Fig. 11. As the expansion coefficients $p_n^{(i)}$ are plural, the norm is used in this computation. Thus, all the physical field quantity (u_x, u_z, T) are positive in this section. It is found from Fig. 11 that: (a) although the piezoelectric effect is weak on thermal wave dispersion and attenuation curves, it is clear on their physical field distributions. The temperature without an electric field is larger than that with an electric field; (b) piezoelectric effects on temperature of A0, S0 and thermal modes are remarkable, especially on the S0 mode with an open-circuit condition; (c) the piezoelectric effect on stresses of A0 and S0

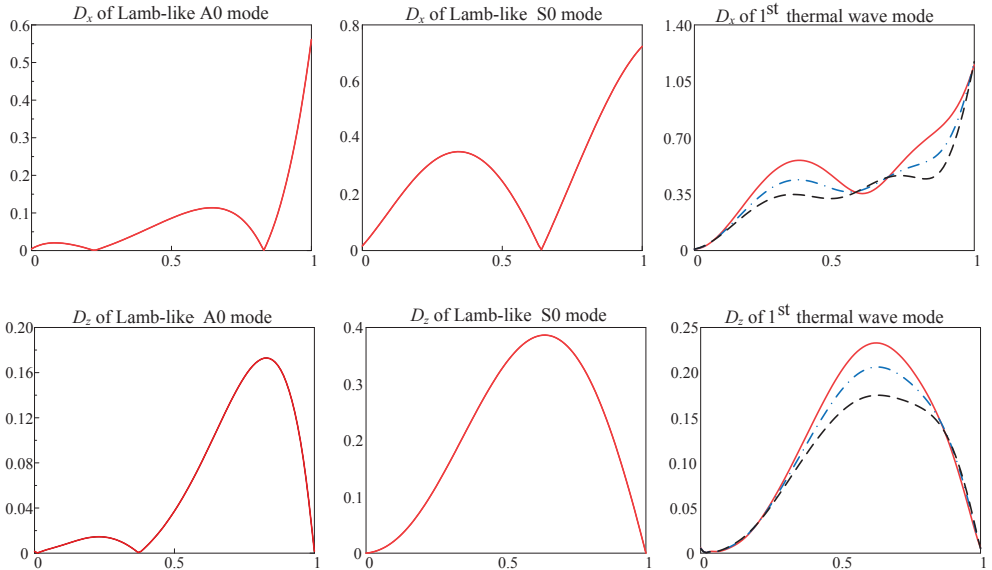


FIG. 13. Influence of relaxation time on electric displacements, $\Omega = 2$;

— $\tau_0 = 1$, --- $\tau_0 = 2$, - · - · $\tau_0 = 3$.

modes is evident. On the whole, the piezoelectric effect has a significant influence on the distribution of physical fields, especially on those with open circuit conditions.

3.4. Relaxation time on physical fields

Finally, the influence of relaxation time on physical field distributions is exhibited with dimensionless $\tau_0 = 1, 2, 3$ in Figs. 12–13. The dimensionless frequency $\Omega = 2$. The A0 and S0 modes and the 1st thermal wave mode with open circuit condition are considered here. Results show that only the stresses of thermal wave mode are affected clearly in Fig. 12, which is similar to the open results [29]. Meanwhile, Fig. 13 shows that the influence of the relaxation time is remarkable on electric displacements of thermal wave modes, but is little on those of Lamb-like modes. For the thermal wave mode, (a) a smaller relaxation time means a larger electric displacements; (b) the influence is notable in the inner of plate, but is negligible at the surface of plate.

4. Conclusions

In this article, the piezoelectric effect on the thermoelastic Lamb wave is studied by the extended LPSA. The original wave problem is translated to a linear eigenvalue problem, which can directly obtain the complex wave number representing the propagation and attenuation. Based on the LS thermoelectric elasticity theory, the following conclusions can be found:

(1) The piezoelectric effect mainly affects the dispersion and attenuation characteristics of Lamb-like waves. The effects on attenuation with the open and closed circuit conditions are consistent for the S0 and S1 modes, but are inconsistent for the A0 and A1 modes.

(2) The attenuation trends of fundamental modes (A0, S0 and the 1st thermal modes) are almost inconsistent with their dispersion curves with $L = 1$ and 2, but those of higher modes (A1, S1 and the 2nd thermal modes) are consistent with their dispersion curves for most frequencies.

(3) The piezoelectric effect is significant on the physical field distributions of thermoelastic Lamb waves, although it is weak on the thermal wave dispersion and attenuation curves. Meanwhile, the piezoelectric effect on temperature of A0, S0 modes are also notable.

(4) The relaxation time has prominent effects on electric displacements of thermal wave modes, but has little effects on those of Lamb-like mode. A smaller relaxation time means a larger electric displacements for the thermal wave mode. In addition, the influence is notable in the inner part of a plate, but is negligible at the surface of a plate.

Appendix A

Defining

$$\begin{aligned}
 u[n, m, j, p] &= \int_{-1}^1 \left(\frac{2z-h}{h} \right)^j Q_n(z) \frac{d^p}{dz^p} Q_m(z) dz, \\
 v[n, m, j, p] &= \int_{-1}^1 \left(\frac{2z-h}{h} \right)^j Q_n(z) \frac{d^p}{dz^p} Q_m(z) \frac{\partial \pi(z)}{\partial z} dz, \\
 t[n, m, j, p] &= \int_{-1}^1 \left(\frac{2z-h}{h} \right)^j Q_n(z) \frac{d^p}{dz^p} [z(z-h)Q_m(z)] \frac{\partial \pi(z)}{\partial z} dz, \\
 s[n, m, j, p] &= \int_{-1}^1 \left(\frac{2z-h}{h} \right)^j Q_n(z) \frac{d^p}{dz^p} [z(z-h)Q_m(z)] dz.
 \end{aligned}$$

The matrices in Eq. (2.17) are given here:

$$\begin{aligned}
 A_{11}^{n,m} &= -C_{11}^{(j)} u[n, m, j, 0], \\
 B_{12}^{n,m} &= i(C_{13}^{(j)} + C_{55}^{(j)})u[n, m, j, 1] + iC_{55}^{(j)}v[n, m, j, 0] + i\frac{2j}{h}C_{55}^{(j)}u[n, m, j-1, 0], \\
 B_{14}^{n,m} &= i(e_{31}^{(j)} + e_{15}^{(j)})u[n, m, j, 1] + ie_{15}^{(j)}v[n, m, j, 0] + i\frac{2j}{h}e_{15}^{(j)}u[n, m, j-1, 0], \\
 B_{13}^{n,m} &= -i\beta_1^{(j)}u[n, m, j, 0], \\
 C_{11}^{n,m} &= C_{55}^{(j)}u[n, m, j, 2] + C_{55}^{(j)}v[n, m, j, 1] + \frac{2j}{h}C_{55}^{(j)}u[n, m, j-1, 1], \\
 M_{11}^{n,m} &= -\omega^2\rho^{(j)}u[n, m, j, 0], \\
 A_{22}^{n,m} &= -C_{55}^{(j)}u[n, m, j, 0], \\
 A_{24}^{n,m} &= -e_{15}^{(j)}u[n, m, j, 0], \\
 B_{21}^{n,m} &= i(C_{55}^{(j)} + C_{13}^{(j)})u[n, m, j, 1] + iC_{13}^{(j)}v[n, m, j, 0] + i\frac{2j}{h}C_{13}^{(j)}u[n, m, j-1, 0], \\
 C_{22}^{n,m} &= C_{33}^{(j)}u[n, m, j, 2] + C_{33}^{(j)}v[n, m, j, 1] + \frac{2j}{h}C_{33}^{(j)}u[n, m, j-1, 1], \\
 C_{23}^{n,m} &= -\beta_3^{(j)}u[n, m, j, 1] - \beta_3^{(j)}v[n, m, j, 0] - \frac{2j}{h}\beta_3^{(j)}u[n, m, j-1, 0], \\
 C_{24}^{n,m} &= e_{33}^{(j)}u[n, m, j, 2] + e_{33}^{(j)}v[n, m, j, 1] + \frac{2j}{h}e_{33}^{(j)}u[n, m, j-1, 1], \\
 M_{22}^{n,m} &= -\omega^2\rho^{(j)}u[n, m, j, 0],
 \end{aligned}$$

$$\begin{aligned}
A_{33}^{n,m} &= -K_1^{(j)} u[n, m, j, 0], \\
B_{31}^{n,m} &= -\omega\eta(1 - i\omega\tau_0)\beta_1^{(j)} u[n, m, j, 0], \\
C_{32}^{n,m} &= i\omega\eta(1 - i\omega\tau_0)\beta_3^{(j)} u[n, m, j, 1], \\
C_{33}^{n,m} &= K_3^{(j)} (u[n, m, j, 2] + v[n, m, j, 1]), \\
C_{34}^{n,m} &= -i\omega\eta(1 - i\omega\tau_0)P_3^{(j)} u[n, m, j, 1], \\
M_{33}^{n,m} &= -i\omega(1 - i\omega\tau_0)\rho^{(j)} C_e^{(m)} u[n, m, j + m, 0], \\
A_{42}^{n,m} &= -e_{15}^{(j)} u[n, m, j, 0], \\
A_{44}^{n,m} &= \epsilon_{11}^{(j)} u[n, m, j, 0], \\
B_{41}^{n,m} &= i(e_{15}^{(j)} + e_{31}^{(j)})u[n, m, j, 1] + ie_{31}^{(j)}v[n, m, j, 0] + i\frac{2j}{h}e_{31}^{(j)}u[n, m, j - 1, 0], \\
B_{43}^{n,m} &= iP_1^{(j)}u[n, m, j, 0], \\
C_{42}^{n,m} &= e_{33}^{(j)}u[n, m, j, 2] + e_{33}^{(j)}v[n, m, j, 1] + \frac{2j}{h}e_{33}^{(j)}u[n, m, j - 1, 1], \\
C_{43}^{n,m} &= P_3^{(j)}u[n, m, j, 1] + P_3^{(j)}v[n, m, j, 0] + \frac{2j}{h}P_3^{(j)}u[n, m, j - 1, 0], \\
C_{44}^{n,m} &= -\epsilon_{33}^{(j)}u[n, m, j, 2] - \epsilon_{33}^{(j)}v[n, m, j, 1] - \frac{2j}{h}\epsilon_{33}^{(j)}u[n, m, j - 1, 1].
\end{aligned}$$

Appendix B

Only matrices related to electric potential are displayed for that other ones are unchanged:

$$\begin{aligned}
B_{14}^{n,m} &= i(e_{31}^{(j)} + e_{15}^{(j)})s[n, m, j, 1] + ie_{15}^{(j)}t[n, m, j, 0] + i\frac{2j}{h}e_{31}^{(j)}s[n, m, j - 1, 0], \\
A_{24}^{n,m} &= -e_{15}^{(j)}s[n, m, j, 0], \\
C_{24}^{n,m} &= e_{33}^{(j)}s[n, m, j, 2] + e_{33}^{(j)}t[n, m, j, 1] + \frac{2j}{h}e_{33}^{(j)}s[n, m, j - 1, 1], \\
C_{34}^{n,m} &= -i\omega\eta(1 - i\omega\tau_0)P_3^{(j)}s[n, m, j, 1], \\
A_{44}^{n,m} &= \epsilon_{11}^{(j)}s[n, m, j, 0], \\
C_{44}^{n,m} &= -\epsilon_{33}^{(j)}s[n, m, j, 2] - \frac{2j}{h}\epsilon_{33}^{(j)}s[n, m, j - 1, 1].
\end{aligned}$$

Acknowledgements

This work was supported by the National Natural Science Foundation of China (No. 51975189), the Project funded by China Postdoctoral Science Foun-

dation (No. 2021M701102), the Key Scientific and Technological Project of Henan Province (No. 222102220037 and 222102230004), the Key discipline of Mechanical Engineering in Henan Polytechnic University, the Innovative research team of Henan Polytechnic University (No.T2022-4), and the Henan University Science and Technology Innovation Team Support Plan (No. 23IRTSTHN016).

Conflict of Interest

The authors declare that they have not known competing financial interests or personal relationships that could have appeared to influence the work reported in this paper.

References

1. S. BRISCHETTO, E. CARRERA, *Refined 2D models for the analysis of functionally graded piezoelectric plates*, Journal of Intelligent Material Systems and Structures, **20**, 15, 1783–1797, 2009.
2. Z. SU, G.Y. JIN, T.G. YE, *Electro-mechanical vibration characteristics of functionally graded piezoelectric plates with general boundary conditions*, International Journal of Mechanical Sciences, **138**, 42–53, 2018.
3. M. AREFI, E.M.R. BIDGOLI, R. DIMITRI, M. BACCIOCCHI, F. TORNABENE, *Application of sinusoidal shear deformation theory and physical neutral surface to analysis of functionally graded piezoelectric plate*, Composites Part B-Engineering, **151**, 35–50, 2018.
4. M.K. PAL, A.K. SINGH, *On the characteristics of reflected waves in rotating functionally graded Initially stressed piezoelectric-orthotropic half-space*, Waves in Random and Complex Media, 1–15, 2021, doi: 10.1080/17455030.2021.1892239.
5. J.H. GUO, J.Y. CHEN, E.N. PAN, *A three-dimensional size-dependent layered model for simply-supported and functionally graded magnetoelastoelectric plates*, ACTA Mechanica Sinica, **31**, 5, 652–671, 2018.
6. P. KUMAR, S.P. HARSHA, *Vibration response analysis of PZT-4/PZT-5H based functionally graded tapered plate subjected to electro-mechanical loading*, Mechanics Research Communications, **116**, 7, 103765, 2021.
7. J. LU, C. YU, W. XU, C. CHIU, *Characteristic orthogonal polynomials-Ritz method for vibration behavior of functionally graded piezoelectric plates using FSDT*, Computers & Mathematics with Applications, **98**, 157–168, 2021.
8. X.T. HE, Y.Z. WANG, S.J. SHI, J.-Y. SUN, *An electroelastic solution for functionally graded piezoelectric material beams with different moduli in tension and compression*, Journal of Intelligent Material Systems and Structures, **29**, 81649–81669, 2018.
9. L. SATOR, V. SLADEK, J. SLADEK, *Analysis of coupling effects in FGM piezoelectric plates by a meshless method*, Composite Structures, **244**, 112256, 2020.
10. R. ANSARI, J. TORABI, M.F. SHOJAEI, *Buckling analysis of axially-loaded functionally graded carbon nanotube-reinforced composite conical panels using a novel numerical variational method*, Composite Structures, **157**, 398–411, 2016.

11. J. TORABI, R. ANSARI, R. HASSANI, *Numerical study on the thermal buckling analysis of CNT-reinforced composite plates with different shapes based on the higher-order shear deformation theory*, *European Journal of Mechanics - A/Solids*, **73**, 44–160, 2019.
12. M. KOMIJANI, J.N. REDDY, A. FERREIRA, *Nonlinear stability and vibration of pre/post-buckled microstructure-dependent FGPM actuators*, *Meccanica*, **49**, 11, 2729–2745, 2014.
13. K. ZHOU, Z.M. HU, H.X. HUA, *Investigation on the nonstationary stochastic response of functionally graded piezoelectric material plates with general boundary conditions*, *Applied Mathematical Modelling*, **96**, 315–335, 2021.
14. A. NOROUZZADEH, R. ANSARI, H. ROUHI, *Nonlinear wave propagation analysis in Timoshenko nano-beams considering nonlocal and strain gradient effects*, *Meccanica*, **53**, 3415–3435, 2018.
15. X. GUO, P.J. WEI, L. LI, M. LAN, *Effects of functionally graded interlayers on dispersion relations of shear horizontal waves in layered piezoelectric/piezomagnetic cylinders*, *Applied Mathematical Modelling*, **55**, 569–582, 2018.
16. H. EZZIN, B. WANG, Z.H. QIAN, *Propagation behavior of ultrasonic Love waves in functionally graded piezoelectric-piezomagnetic materials with exponential variation*, *Mechanics of Materials*, **148**, 103492, 2020.
17. M.S. CHAKI, A.K. SINGH, *The impact of reinforcement and piezoelectricity on SH wave propagation in irregular imperfectly-bonded layered FGPM structures: an analytical approach*, *European Journal of Mechanics - A/Solids*, **80**, 103872, 2020.
18. C.L. LI, Q. HAN, *Guided waves propagation in sandwich cylindrical structures with functionally graded graphene-epoxy core and piezoelectric surface layers*, *Journal of Sandwich Structures and Materials*, **23**, 8, 3878–3901, 2020.
19. B. ZHANG, X.H. WANG, L. ELMAIMOUNI, J.G. YU, X.M. ZHANG, *Axial guided wave characteristics in functionally graded one-dimensional hexagonal piezoelectric quasi-crystal cylinders*, *Mathematics and Mechanics of Solids*, **27**, 1, 125–143, 2021.
20. B. ZHANG, J.G. YU, X.M. ZHANG, P.M. MING, *Complex guided waves in functionally graded piezoelectric cylindrical structures with sectorial cross-section*, *Applied Mathematical Modelling*, **63**, 288–302, 2018.
21. H. EZZIN, M. MKAOIR, M. AREFI, Z. QIAN, R. DAS, *Analysis of guided wave propagation in functionally graded magneto electro elastic composite*, *Waves in Random and Complex Media*, 1–19, 2021.
22. Y. HEYDARPOUR, P. MALEKZADEH, R. DIMITRI, F. TORNABENE, *Thermoelastic analysis of functionally graded cylindrical panels with piezoelectric layers*, *Applied Sciences (Basel)*, **10**, 4, 1397, 2020.
23. P.K. SAROJ, S.A. SAHU, S. CHAUDHARY, A. CHATTOPADHYAY, *Love-type waves in functionally graded piezoelectric material (FGPM) sandwiched between initially stressed layer and elastic substrate*, *Waves in Random and Complex Media*, **25**, 4, 608–627, 2015.
24. P. LI, F. JIN, X.S. CAO, *Investigation of trapped thickness-twist waves induced by functionally graded piezoelectric material in an inhomogeneous plate*, *Smart Materials & Structures*, **22**, 9, 095021, 2013.
25. V. SHARMA, S. KUMAR, *Analysis of size dependency on Love-type wave propagation in a functionally graded piezoelectric smart material*, *Mathematics and Mechanics of Solids*, **25**, 8, 1517–1533, 2020.

26. C.X. XUE, E. PAN, *On the longitudinal wave along a functionally graded magneto-electro-elastic rod*, International Journal of Engineering Science, **62**, 48–55, 2013.
27. M. MOHAMMADI, M. BAMDAD, K.A. LAMBEIGI, R. DIMTRI, F. TORNABENE, *Electro-elastic response of cylindrical sandwich pressure vessels with porous core and piezoelectric face-sheets*, Composite Structures, **225**, 111–119, 2019.
28. J.G. YU, B. WU, G.Q. CHEN, *Wave characteristics in functionally graded piezoelectric hollow cylinders*, Archive of Applied Mechanics, **9**, 807–824, 2009.
29. X.H. WANG, F.L. LI, X.M. ZHANG, J. YU, H. QIAO, *Thermoelastic guided wave in fractional order functionally graded plates: An analytical integration Legendre polynomial approach*, Composite Structures, **256**, 7, 112997, 2021.
30. J.N. SHARMA, M. PAL, *Propagation of Lamb waves in a transversely isotropic piezothermoelastic plate*, Journal of Sound & Vibration, **270**, 4–5, 587–610, 2004.
31. C.C. LIU, J.G. YU, W.J. XU, *Theoretical study of elastic wave propagation through a functionally graded micro-structured plate base on the modified couple-stress theory*, Meccanica, **55**, 5, 11531167, 2020.
32. C. OTHMANI, H. ZHANG, C.F. LÜ, Y.Q. WANG, A.R. KAMALI, *Orthogonal polynomial methods for modeling elastodynamic wave propagation inelastic, piezoelectric and magneto-electro-elastic composites – a review*, Composite Structures, **286**, 115245, 2022.
33. M.F. ZHENG, H.W. MA, Y. LYU, C. LU, C. HE, *Derivation of circumferential guided waves equations for a multilayered laminate composite hollow cylinder by state-vector and Legendre polynomial hybrid formalism*, Composite Structures, **255**, 112950, 2020.
34. J.E. LEFEBVRE, J.G. YU, F.E. RATOLOJANAHARY, *Mapped orthogonal functions method applied to acoustic waves-based devices*, AIP Advances, **6**, 6, 065307, 2016.
35. X.S. CAO, J. FENG, I. JEON, *Calculation of propagation properties of Lamb waves in a functionally graded material (FGM) plate by power series technique*, NDT & E International, **44**, 1, 84–92, 2011.
36. M.B. AMOR, I.B. SALAH, M. GHOZLEN, *Propagation behavior of Lamb waves in functionally graded piezoelectric plates*, Acta Acustica United with Acustica, **101**, 3, 435–442, 2015.
37. H. AL-QAHTANI, S. DATTA, *Thermoelastic waves in an anisotropic infinite plate*, Journal of Applied Physics, **96**, 7, 3645–3658, 2004.
38. S. GUHA, A.K. SINGH, *Plane wave reflection/transmission in imperfectly bonded initially stressed rotating piezothermoelastic fiber-reinforced composite half-spaces*, European Journal of Mechanics – A/Solids, **88**, 104242, 2021.

Received June 2, 2022; revised version October 20, 2022.

Published online February 15, 2023.
